BioBased Piezo and Thermoresistive Photocurable Sensing Materials from Acrylated Epoxidized Soybean Oil

Bio-based Piezo- and Thermo-Resistive Photo-Curable Sensing Materials from Acrylated Epoxidized Soybean Oil

Cristian Mendes-Felipe, Pedro Costa, Ignazio Roppolo, Marco Sangermano, Senentxu Lanceros-Mendez*

C. Mendes-Felipe, S. Lanceros-Mendez
BCMaterials, Basque Center for Materials, Applications and Nanostructures, UPV/EHU Science Park, 48940 Leioa, Spain
E-mail: cristian.mendes@bcmaterials.net

P. Costa
Center of Physics, University of Minho, Campus de Gualtar, 4710-057 Braga, Portugal

P. Costa
Institute for Polymers and Composites IPC, University of Minho, 4804-533 Guimarães, Portugal

I. Roppolo
Center for Sustainable Future Technologies, Istituto Italiano di Tecnologia, Via Livorno 60, 10144 Torino, Italy

C. Mendes-Felipe, I. Roppolo, M. Sangermano
Dipartimento di Scienza Applicata e Tecnologia (DISAT), Politecnico di Torino, C.so Duca Degli Abruzzi 24, 10129, Torino, Italy

S. Lanceros-Mendez
Ikerbasque, Basque Foundation for Science, 48009 Bilbao, Spain

Keywords: Bio-based resins, Reduced graphene oxide, Polymer composites, UV-curing, Piezoresistive

Bio-based photocurable polymers are increasingly demanded as environmentally friendly materials for advanced applications. Together with functional fillers, represent a next step for

the generation of functional and active smart materials, compatible with additive manufacturing technologies. This work reports on, acrylated epoxidized soybean oil (AESO) mixed with different amounts of reduced graphene oxide (rGO) up to 6 wt.% in order to obtain UV-curable piezoresistive and thermoresistive materials. It is shown that the addition of rGO to AESO hinders the curing process, but maintains always double bond conversions higher than 50 %. Composites are characterized by a good dispersion of micrometric filler clusters. Further, the thermal stabilities are close to 300ºC and cross-linking degrees are above 1.75 mmol·cm^{-3}. The Young modulus of the composites decreases with the addition of the rGO fillers, in particular for the higher filler contents, and electrical conductivities up to 0.13 S·m^{-1} are obtained for the composites with the highest rGO content. UV-curable composites with piezoresistive and thermoresistive responses suitable for applications are thus obtained, characterized by gauge factors around 26 for deformations up to 2% and maximum thermoresistive sensitivity of S = 0.43, similar values to the values obtained for petroleum-based materials.

1. Introduction

Research and technological development are increasingly focusing on smart and multifunctional materials.[1] The current demands of the Industry 4.0 concept are based on the necessity to control any process at any time,[2] in relation to the "Internet of Things".[3] In this sense, the use of sensors and actuators plays an essential role in industry development,[4] as well as in areas such as health monitoring,[5] aerospace and automotive applications,[6] gas detection,[7] agriculture and the food industry.[8]

An increasing number of daily used sensors and actuators are polymer-based smart materials.[9] Herein, polymer composites highlight due to the synergistic combination of their inorganic and organic constituents. In this approach, the polymer matrix provides processability advantages such as flexibility or ductility, while the nanofillers typically allow to tune or induce specific physico-chemical properties, such as magnetism, optical properties or electrical conductivity.[10] These polymer composites can be prepared by different methods, including solvent casting or from the melting,[11] but photopolymerization, defined as a polymerization reaction that rapidly converts liquid formulations containing oligomers, monomers and photoinitiator into a solid polymer by irradiation with light, emerges as one of the most suitable alternatives. In fact, it presents a series of advantages, such as reduced emission of volatile organic compounds, fast curing or improved accuracy of the printed patterns without the use of solvents and high temperatures, which reduces the environmental impact of the polymer processing.[12]

Typically, the thermoset polymers employed in the photopolymerization process are based on multifunctional acrylates derived from crude oil, raising concerns regarding their environmental impact.[13] Thus, accordingly to the European Green Deal and Circular Economy policies,[14] renewable feedstock materials are increasingly explored nowadays, including for UV-curable materials.[15] In fact, the consumption of non-renewable energy and the carbon dioxide emission can be reduced through the use of natural-based materials, being bio-based thermoplastics widely available but bio-based thermosets still limited, representing thus an interesting and urgent challenge for materials research.[16]

The use of renewable resources for the production of thermosets polymers are continuously increasing. In this scope, vegetable oils, terpenes and carbohydrates such as soybean, linseed and castor oils, limonene or starch are among the most used monomers for the manufacture of plastics, elastomers or hydrogels.[17] In particular, oils and fats obtained from vegetables or animals are the most important renewable feedstock employed in the synthesis of photocurable bio-based materials, typically, after being functionalized using epoxidation or (meth)acrylation

reactions.[15] Here, soybean oil stands out among the different bio-based polymers as it is one of the vegetable oils, together with palm and rapeseed oils, that presents the largest global production volumes and the most economical prices for large-scale use in commercial products.[18] It is also characterized by good mechanical properties, low curing time in the presence of photoinitiator and high thermal stability,[19] being thus used as a bio-based resin for 3D printing.[20–22]

However, there are just few studies focusing on the photopolymerization of composite materials based on natural sources, mainly due to light absorption and viscosity issues that hinder a proper and efficient curing process.[23] As examples, urethane acrylate pre-polymer has been synthesized with castor oil and mixed with modified zinc oxide nanoparticles to increase its glass transition temperature.[24] Acrylated epoxidized linseed oil has been also used together with anatase titanium dioxide nanoparticles for the preparation of mechanically reinforced coatings with antimicrobial behavior.[25] Organic fillers have been also used as fillers such as micro-scale bamboo fibers for the reinforcement of palm oil-based thermosets composites,[26] synthetic nylon fibers within resorcinol epoxy acrylate oligomer[27] or microfibrillated cellulose with epoxidized cardanol.[28] In addition, conventional photocurable polymeric matrices like poly(ethylenglycol) diacrylate has been reinforced with fillers of natural origin like pollen.[29]

With respect to nanofillers for the processing of smart polymer composites, carbon-based materials, namely carbon nanotubes, carbon black or graphene oxide, are particularly suitable for developing multifunctional sensing materials, as they present thermal stability, low toxicity, flexibility and high electrical and thermal conductivities.[30,31] Polymer-based composites containing carbonaceous materials have been widely used in applications such as temperature, humidity, pressure or deformation sensors.[32] In particular, different functional systems and devices have been prepared based on piezoresistive and thermoresistive materials obtained by the combination of carbon-based fillers and different thermoplastic polymers,[33,34] at the point that the use of carbonaceous materials in combination with photocurable systems have been extended to 3D printing[35] or even 4D printing.[36] However, despite these recent advances and up to our knowledge, there are not cases in which carbon-based fillers have been combined with UV curable bio-based resins in order to obtain piezoresistive and/or thermoresistive materials with improved sustainability, addressing therefore, both the functional and environmental needs of current society.

In this scope, this work demonstrates the development of stimuli responsive materials obtained via photopolymerization of a natural-based polymer composite. Acrylated epoxidized soybean oil (AESO) was used as a matrix and reduced graphene oxide (rGO) as a functional filler. The

developed material showed piezoresistive and thermoresistive responses, that were characterized together with a physico-chemical properties, as a function of rGO content.

2. Results and Discussion

2.1. UV-Curing Process

The photopolymerization processability of the different formulations was evaluated by real-time photorheology, measuring the evolution of both storage and loss moduli (G' and G'', respectively) while samples were irradiated with UV-light at 405 nm. The G' values as a function of time *(t)* for all samples are reported in **Figure 1**a. The curing rate ($\Delta G'/\Delta t$) measured as the slope of the curve in the initial irradiation times, and the gel time (t_{gel}) or time required to reach the crossover between both moduli are obtained and collected in **Table 1**.

The photorheology curves show that all samples can be cured by UV light, independently of the rGO content, as identified by the plateau observed in all of them. However, the presence of carbonaceous filler affects the photopolymerization reaction, leading to an increase of the gel time and to a slower kinetics when the rGO content increases, as revealed by the decreased slopes of the G' curves. In particular, t_{gel} increases from 17.8 ± 1.1 to 79.8 ± 5.2 s by increasing rGO content in the precursor formulation from 0 to 6 wt.%, while the curing rate is slowed down from 75.5 ± 7.5 to 0.07 ± 0.02 $kPa.s^{-1}$, respectively.

The lower photoreactivity of the formulation with increasing rGO content is thus ascribed to the UV-light shielding effect of graphene. A lower amount of reactive species is photogenerated due to the light absorption by the rGO which competes with the light absorption by the photoinitiator, resulting in a decrease of the acrylic double bond conversion and, therefore, to a slowed photopolymerization rate.[37] A similar effect has been reported in literature for rGO dispersed into UV-curable epoxy resins.[38] Furthermore, the increased G' values of the formulations containing rGO before the onset of photopolymerization indicate an increase in the viscosity of the formulations, which is clearly observed during the preparation of the samples.[36]

The photopolymerization process was also characterized by FTIR, measuring the acrylic double bond (C=C) conversion upon samples irradiation under nitrogen atmosphere. The average percentages of conversion were calculated monitoring the decrease of the corresponding peak centered at 1630 cm^{-1},[39] and the obtained data for all formulations are reported in Table 1. Figure 1b shows the FTIR spectra and the acrylic double bond conversion of the neat polymer as a representative example.

The FTIR spectra of AESO displays the characteristic peaks associated to the main functional groups of the polymer. The stretching vibrations of -OH groups, C=O and C-O-C group of ester are shown at 3460, 1730 and 1160 cm^{-1}, respectively. Also, the bands at 2920, 2850 and 1450 cm^{-1} can be identified and are due to the asymmetric stretching vibrations and deformations of the C-H bond in the $-CH_2-$ and $-CH_3-$ groups. In addition, the presence of the C=C band is corroborated by the peak located at 1630 cm^{-1}.[39]

The success of the acrylic double bond conversion was confirmed by the decrease of the peak centered at 1630 cm^{-1} upon irradiation.[40] The presence of rGO affected the conversion of double bonds with a decrease of percentage of conversion by increasing rGO content in the photocurable formulation (Table 1), in accordance with the photorheology data. When the rGO content increases, a decrease in the conversion is clearly observed and it is significative higher for the samples with the highest rGO content, i.e. 5 and 6 wt.%. For those samples, the apparent viscosity appreciated during formulations preparation can represent an additional factor hindering the photopolymerization process.[37]

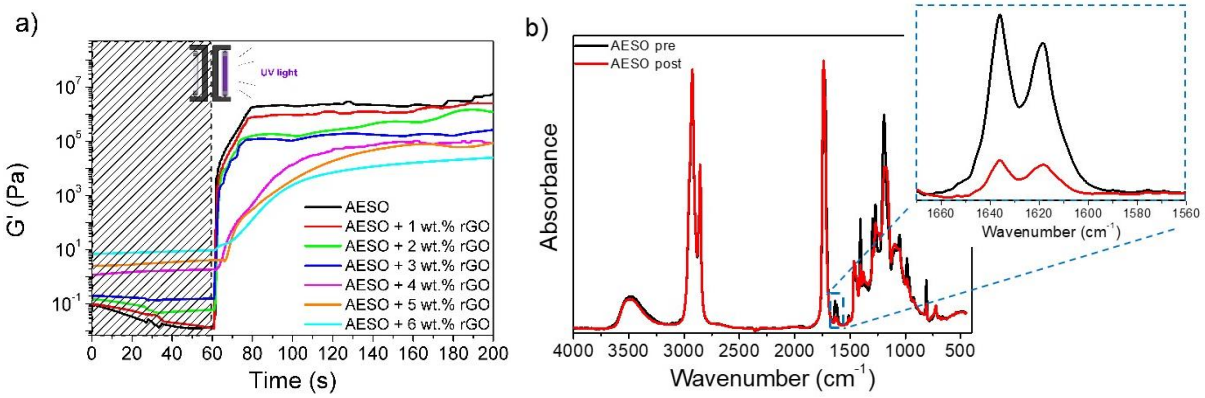

Figure 1. a) Photorheologhy curves corresponding to the photopolymerization of AESO and their composites with different rGO contents. b) FTIR spectra for AESO before (pre) and after (post) irradiation with UV-light showing the double bond conversion.

Table 1. Photopolymerization main characteristics of AESO and AESO/rGO composites.

Sample	t_{gel} (s)	$\Delta G'/\Delta t$ (kPa s^{-1})	FTIR conversion (%)
AESO	17.8 ± 1.1	75.5 ± 7.5	70 ± 2
AESO + 1 wt.% rGO	18.1 ± 1.3	29.8 ± 3.2	68 ± 3
AESO + 2 wt.% rGO	19.3 ± 1.5	7.0 ± 0.5	69 ±5
AESO + 3 wt.% rGO	19.8 ± 2.5	6.3 ± 0.6	67 ± 3
AESO + 4 wt.% rGO	40.7 ± 4.7	0.31 ± 0.08	63 ± 4
AESO + 5 wt.% rGO	68.6 ± 4.9	0.15 ± 0.03	51 ± 5
AESO + 6 wt.% rGO	79.8 ± 5.2	0.07 ± 0.02	45 ± 7

2.2. Morphological Characteristics

Filler dispersion and wettability between the rGO and the AESO were evaluated by SEM images analysis of thin film samples with different filler contents. **Figure 2** shows the SEM images of pristine and rGO dopped samples at different magnifications.

The rGO dispersion within the polymer matrix can be identified as white platelets in the SEM images,[33,41,42] the composite materials presenting quite different appearance compared with AESO neat polymer, which is a completely flat material without any voids or loose interfaces. When rGO is added, the appearance of white agglomerates of several micrometers is observed, that increase in number when rGO content increases. Thus, there is no individual dispersion of rGO within the polymer matrix, but a good distribution of small clusters, which is preferred to achieve higher electrical conductivities, while maintaining suitable mechanical properties.[43,44] Further, filler contents above 4 wt.% lead to the appearance of some voids within the polymer matrix, that can have an impact in the mechanical properties, as it will be discussed later. However, it is to stress that the obtained aggregates are homogeneously dispersed along the samples, even in the case of higher filler contents (6 wt.% rGO) and that just a limited number of small voids is observed, not compromising the electrical characteristics and the mechanical integrity of the samples (section 2.4.).

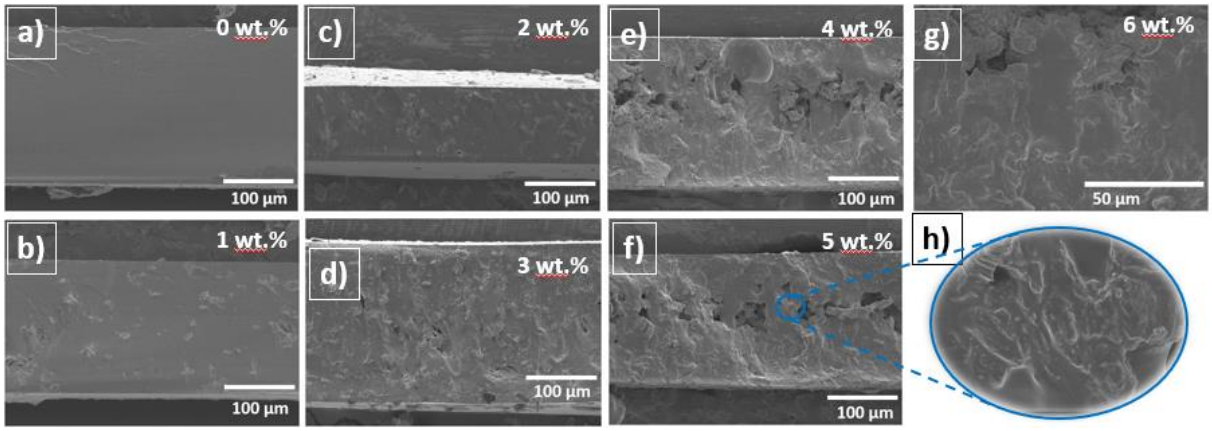

Figure 2. Representative SEM images of AESO/rGO composites for filler contents ranging from 0 to 6 wt.% at magnifications of 300× (a-f), 1000× (g) and 3000×(h).

2.3. Thermal and Viscoelastic Properties

Thermal properties of AESO/rGO composites were studied by thermogravimetric analysis (TGA) and differential scanning calorimetry (DSC) to define thermal decomposition behavior and glass transition temperatures ($T_{g\text{-}DSC}$), respectively.

As **Figure 3**a shows, the thermal degradation process of both AESO and AESO/rGO composites mainly occurs in one step, as identified by a single mass-loss stage between 300 and 460 °C, corresponding to the degradation of AESO chains.[45] In addition, all prepared materials show the thermal decomposition temperature at the weight loss of 5% ($T_{d\text{-}5\%}$) above

275ºC (Figure 3a inset). Samples with higher rGO contents present significantly low $T_{d\text{-}5\%}$ values, being approximately 310 ºC for neat AESO and AESO/rGO composites up 4 wt.% filler content, decreasing down to 295 and 290 ºC for 5 and 6 wt.% rGO content samples, respectively. This can be ascribed to the differences in the photopolymerization process, the higher rGO content hinders the curing process achieving a less crosslinked materials with a slightly lower thermal stability.[37]

DSC analysis was used to evaluate the evolution of $T_{g\text{-}DSC}$ of AESO/rGO composites with increasing filler content (Figure S1) and **Table 2** indicates the obtained $T_{g\text{-}DSC}$ values. It is found that the addition of rGO to AESO do not significantly alter the $T_{g\text{-}DSC}$ of the cured films, being just observed a decrease for high rGO contents, associated to a flexibilization of the polymer network due to the crosslinking degree reduction induced by the UV-shielding effect of rGO, as previously discussed. However, this effect is low due to the small amount of the filler added that is unable to strongly influence the mobility of the polymer chains,[46] similarly results were reported in literature when rGO is used as filler in photopolymerization of poly (ethylenglycol) diacrylate (PEGDA).[47]

Thermal and viscoelastic properties of AESO and AESO/rGO composites were fully characterized by dynamic mechanical thermal analysis (DMTA), in order to obtain the storage (E') and loss (E'') modulus, and the corresponding glass transition temperature of DMTA ($T_{g\text{-}DMTA}$) conventionally defined as the peak observed on the tan δ curve (tan δ = E''/E').

It is possible to observe that all curves present similar shapes and are of the same magnitude, independently on the filler content. Attending to the $T_{g\text{-}DMTA}$ values, a decrease is observed when rGO content increases, denoted by a short shift on the maximum of tan δ curves toward lower temperature, from 26 ºC of AESO neat polymer to 0 ºC for the 4 wt.% AESO/rGO sample (Table 2). This is in accordance with the DSC results. The $T_{g\text{-}DMTA}$ values are higher than $T_{g\text{-}DSC}$ ones due to the different time response of the measurement (frequency effect).[48] Samples containing 5 and 6 wt.% rGO are not possible to be measured by DMTA due to the instable properties of the cured samples that induces an early break during characterization. Finally, the tan δ curves of AESO/rGO composites as a function of temperature are slightly broader (with exception of 4 wt.% sample) than the one of the AESO pristine sample, suggesting a more heterogenous network for composites materials.[49]

Observing to the E' values, all samples present a single E' step decrease that change from around $0.7–1 \times 10^9$ Pa to $2–3 \times 10^7$ Pa, corresponding to the transition between the glassy and the rubbery state (glass transition).[48] As it is described in the experimental part, the moduli in the rubbery plateau can be related with the cross-linking density (ν_c) of the polymer networks

and the ν_c values for the different samples are reported in Table 2. The addition of rGO to AESO induces a decrease of ν_c from 3.04 mmol.cm^{-3} in AESO to 1.75 mmol.cm^{-3} for the 4 wt.% rGO content sample. This result agrees with the results of the photopolymerization process which indicate a decrease on the double bond conversion due to the shielding effect of the rGO, with the corresponding decrease of crosslinking points in the polymer network and, therefore, the decrease on cross-linking density.

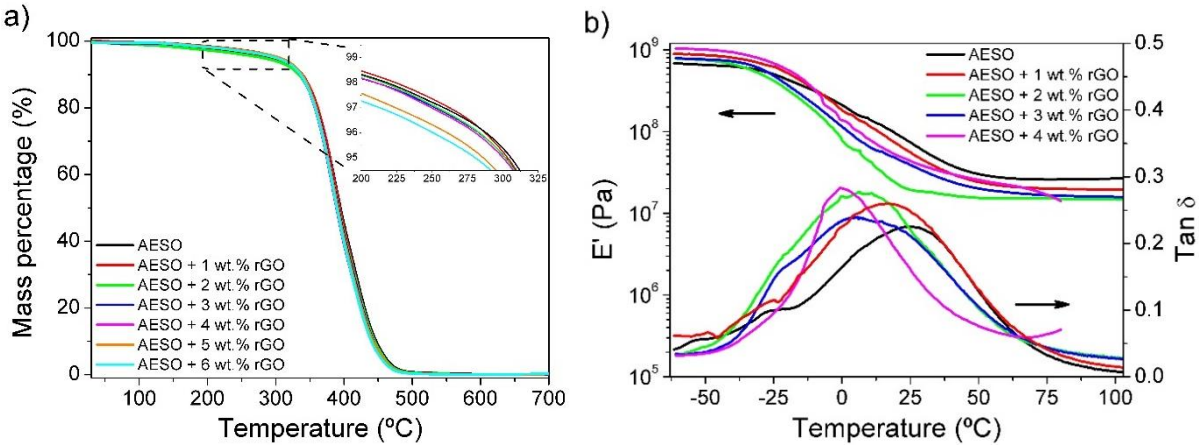

Figure 3. a) Thermal degradation analysis and b) tan δ and E' curves from dynamic mechanical thermal analysis of AESO and AESO/rGO composites for 1 to 6 wt.% rGO content.

2.4. Mechanical and Electrical Properties

The mechanical characterization of the samples was carried out by strain-stress measurements of thin films. In Figure 4 the stress-strain curves are reported for the different investigated samples. The Young modulus (E) and strain at break (ε_b) values for the samples are summarized in Table 2.

The AESO sample presents an E value around 93.9 MPa and the addition of low contents of rGO does not influence this value significantly. The addition of 2 wt.% rGO content induces a slight decrease of E down to 81.5 MPa what is more marked for samples with higher filler content and, in particular, for the sample with 4 wt.% rGO content that presents an E value of 39.1 MPa. This is associated to the negative influence of the addition of rGO in the curing process as evidenced in photorheology analyses (plateau values) and ATR-FTIR experiments.[47] The addition of a highly light absorbing filler reduces the photogeneration of reactive species and this competition between the photoinitiator and the filler leads to a less effective curing process and, therefore, to a lower crosslinked material.[50] In addition, the deterioration of mechanical properties of the polymer containing carbonaceous material can be also related to the presence of filler agglomerated, as evidenced in the SEM images, which act

as defects, leading to heterogeneous stress distributions during the stress-strain measurements.[37]

At higher strains, the stress increases nearly linear with the strain up to the breaking of the film. The maximum strain that films can stand before breaking, named as strain at break (ε_b), varies from 6.6% for the neat polymer to 4.7% for the sample containing 4 wt.% rGO. Samples with 5 and 6 wt.% filler content were unable to be measured due to the inhomogeneity of the samples (filler agglomerations, voids or defects) and that causes an early break.

The effect of filler addition in the photopolymerization process is also related to the decrease of the elongation of the AESO polymer chains due to particle-polymer interactions that restrict the segmental motion of the polymer and, therefore, decrease the maximum elongation values in the composite samples.[51]

Regarding the electrical response of the prepared materials, Figure 4b presents electrical conductivity of the samples as a function of rGO content obtained from the intensity-current (I-V) characteristic curves shown in Figure S2 of the Supporting Information. The percolation threshold determined for AESO/rGO samples is presented as inset in Fig. 4b.

Representative I-V curves of all measured materials show a linear behavior between the measured current and the applied voltage. The addition of rGO leads to an increase of the electrical conductivity as represented by the increase in the slope of the I-V curves.

The electrical conductivity (σ) of the samples is calculated from the slope of the I-V curve and using the Ohm's law. The electrical conductivity of AESO is 8.8×10^{-12} S m^{-1} and the addition of low contents of rGO up to 3 wt.% does not lead to a significantly variation of the electrical conductivity, reaching 2.2×10^{-11} S m^{-1} for the sample with 2 wt.% rGO content. For filler content above 3 wt.% rGO, the electrical conductivity increases in several orders of magnitude, as corresponding to a percolative system.[41,52] The σ values for AESO/rGO samples increase from 2.3×10^{-10} S m^{-1} for the 3 wt.% sample to 0.13 S m^{-1} for the sample with the highest rGO content (6 wt.% samples). Thus, percolation threshold for the AESO/rGO samples is located between 3 wt.% and 5 wt.%.

The calculation of the percolation threshold (Figure 4b, inset) provides the percolation concentration at 4.1 wt.% rGO content, being in the order of the values obtained for related polymer-based composites reported in literature.[42] Further, the universal exponent (t) that depends on the connectivity of conductive material and indicates the dimensionality of the conductive system, and that typically is between 1 and 1.3 for 2D networks and between 1.5 and 2 for 3D networks, shows in the present case the value of 8.5. This can be attributed to the inhomogeneity of the rGO dispersion within the AESO matrix, which is consistent with the

aggregates and voids observed in SEM images (Figure 2), indicating a not perfectly defined 2D or 3D conductive path.[53]

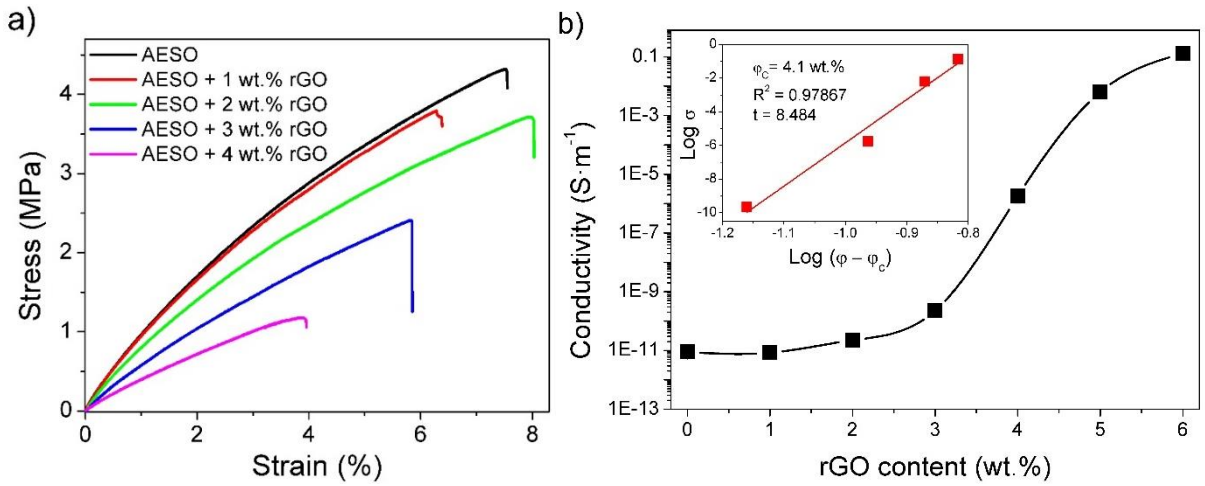

Figure 4. a) Mechanical behavior of AESO and AESO/rGO composites up to 4 wt.% rGO content and b) electrical conductivity as a function of rGO content for composites up to 6 wt.% rGO content, with the determination of theoretical percolation threshold for the composites (inset).

2.5. Piezoresistive and Thermoresistive Properties

The piezoresistive properties of the AESO/rGO composites (**Figure 5**) were evaluated under uniaxial stress mode and the piezoresistive sensitivity (Gauge Factor, GF) was evaluated for samples containing the highest filler content (6 wt.% rGO). The piezoresistive sensibility of polymer composites is typically higher near the percolation threshold (4 wt.% in the present case) but just for low deformations, as large deformations lead to a breakdown of the conductive network of the samples. For large deformation applications, larger filler contents above the percolation threshold are needed.[54]

The electro-mechanical response under loading and unloading cycles for 1% strain deformation is represented in Figure 5a. It is shown that the electrical resistance variation follows the mechanical strain applied to the composites, increasing the electrical resistance with increasing applied strain and *vice versa*. The electrical behavior suffers some relaxation over cycling, indicating that the conductive network does not completely recovers upon strain release, due to irreversible rearrangements of the network.[55] However, a good linear relationship between electrical variations and deformation is observed, allowing the calculation of the GF.[37,56]

The obtained GF are in the range between 20 and 26 for the different applied strains and for the different loading-unloading cycles, excepting for the 0.1% strain that shows a GF value of 6.6 ± 3.5. The increase of applied strain does not imply an increase of the GF as Figure 5c shows,

being therefore compatible with a linear regime. The highest GF value is 25.7 ± 3.1 and was obtained for a strain of 0.5%, being the GF values for the rest of the deformations within experimental error. Similar behavior has been found in rGO/polymer composites with a GF values in the same order of magnitude.[54,57]

The piezoresistive response is determined by two contributions: the intrinsic piezoresistive effect ($\frac{d\rho/\rho_0}{dl/l_0}$) and the geometrical effect ($1 + 2\nu$). Thus, piezoresistive composites with larger GF values than their geometric contribution show relevant intrinsic conductivity variation when stress is applied,[54] i. e., variations of rGO network during sample deformation. In this case, as the Poisson ratio of AESO is around 0.43,[58] the maximum value of the GF that can be associated to the geometrical contribution is $GF_{geometric} \approx 2$, which means that the piezoresistive behavior of AESO/rGO composites is mostly attributed to an intrinsic piezoresistive effect.

The not fully recovery of the conductive network over repeated cycling and the successive generation of a permanent modifications is reflected also in the slight decrease of the resistance maximum and minimum values (Figure 5a).[33] Nevertheless, under repeated stress-strain cycling (over 500 cycles), a stabilization of the maximum and minimum resistance values is observed (Figure 5d), indicating that aging is required to stabilize the piezoresistive response of AESO/rGO composites in order to be applied as quantitative sensing materials. Moreover, the variation of the electrical resistance involves a change in GF values for the initial cycles, remaining constant and nearly around 9 after several cycles as can be observed in Figure 5c. This behavior is typical for polymer-based materials,[34,41] including UV curable piezoresistive ones,[37] and is related to "irreversible reconfigurations of the conductive network" that occurs during the piezoresistive cycling after several number of cycles.

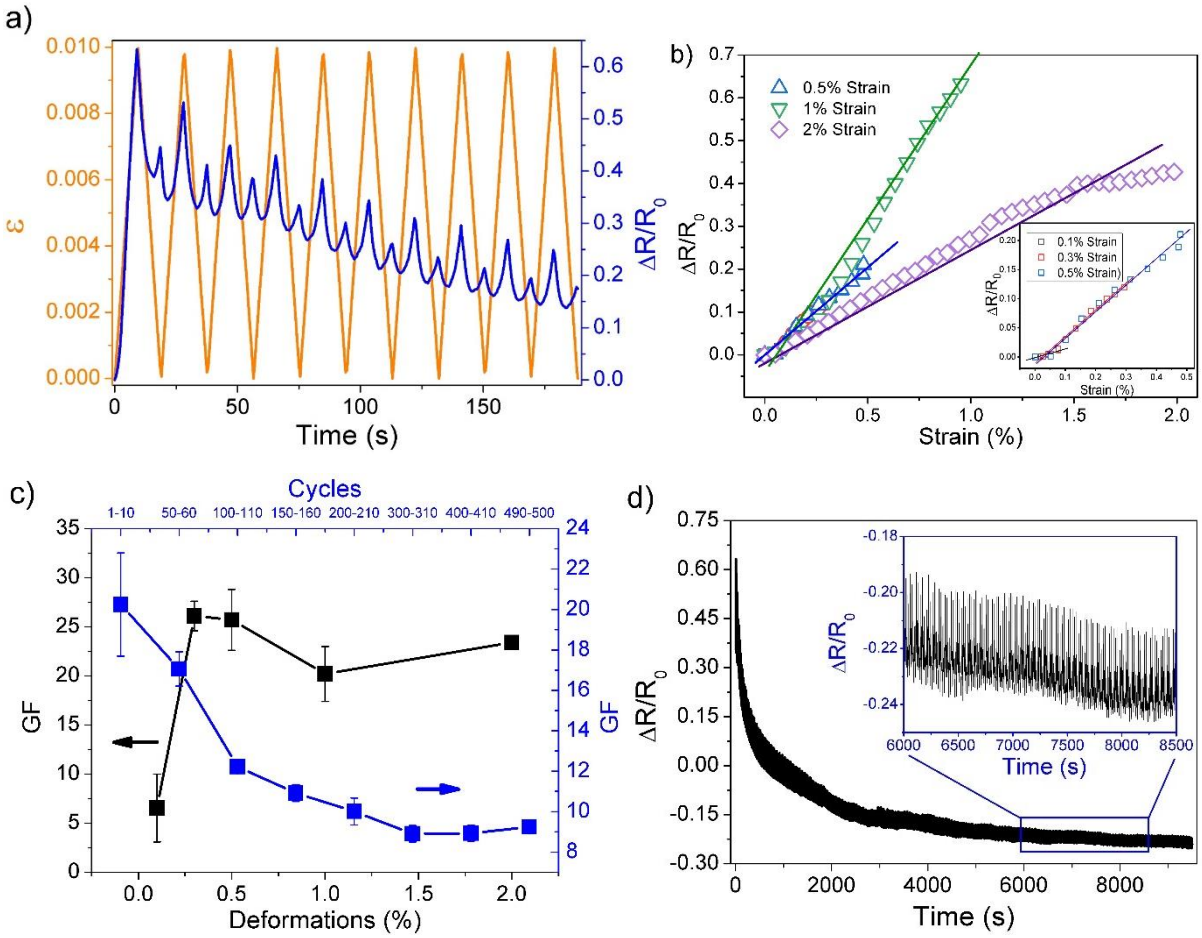

Figure 5. Piezoresistive response of the AESO/rGO composite with 6 wt.% rGO content: a) piezoresistive behavior for 10 stress-strain loading-unloading cycles at 1% strain, b) linear behavior between resistance changes ($\Delta R/R_0$) and strain for the different applied deformations, c) piezoresistive sensibility, Gauge Factor (GF), as a function of deformations and number of cycles for 1% deformation, and d) electromechanical test for 500 cycles at 1% deformation.

The thermoresistive properties of the AESO/rGO composites (**Figure 6**) were evaluated in the samples with the highest filler content, 6 wt.%, in the temperature range from 25 to 50 ºC, suitable for applications in areas such as microelectromechanical systems, medicine, agriculture, food, chemical, and aerospace industries.[59]

Figure 6a demonstrates that the thermoresistive response of the AESO/rGO composites is linear and positive, increasing the electrical resistance with increasing temperature and decreasing with decreasing temperature. The slopes observed for the four heating-cooling cycles show a stable and linear behavior (Figure 6b) with a thermoresistive sensibility (S) –Equation 5, experimental section– of 0.43 ± 0.03 $ºC^{-1}$. This value is in the range of the ones obtained for carbonaceous/polymer composites prepared using carbon nanotubes or graphene in combination with different polymers such as cellulose, polyethyleneoxide and polysulfone.[33,59,60]

The mechanisms that determines the effective thermoresistive response are the intrinsic thermoresistivity of the filler, the thermal expansion/contraction of the polymer, the tunneling effect associated to this expansion/contraction, and filler-filler interactions.[61] Particularly, studies carried out using graphene-based materials had reported quite diverse results including both positive[62] and negative[33] thermal resistivity sensibilities.

Overall, the prepared bio-based UV curable materials from acrylated epoxidized soybean oil show piezoresistive and thermoresistive properties similar to the ones obtained for petroleum-based materials and are compatible with a wide range of applications. Further, considering the UV curing properties obtained, AESO/rGO composites show the ability to be 3D printed by DLP or other UV curing-based 3D printing technologies.

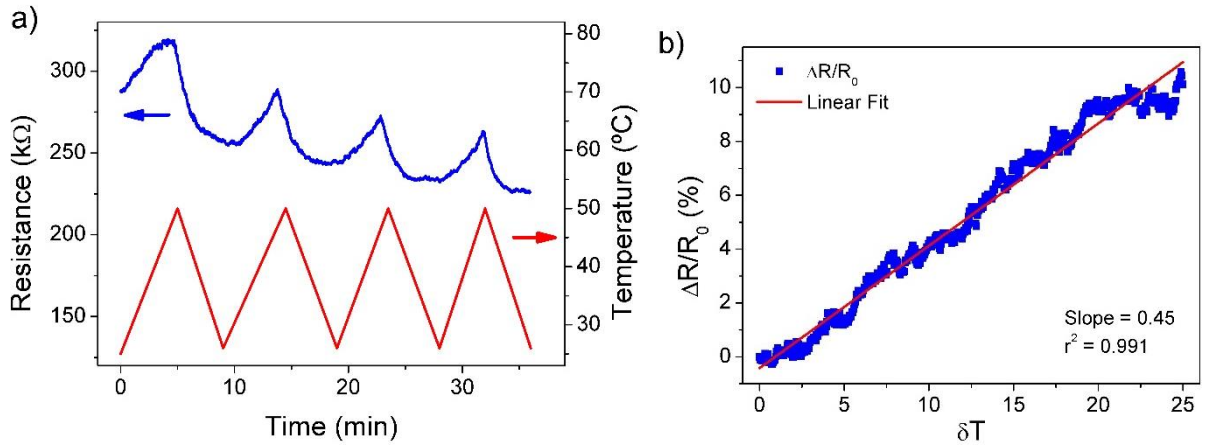

Figure 6. a) Relative resistance variation of AESO/rGO composite with 6wt.% rGO content for the temperature range from 25 to 50 ºC. b) Linearity between the electrical resistance variation and temperature variation.

Table 2. Main properties of the photocured AESO and AESO/rGO composite films.

Sample	$T_{g\text{-}DSC}$ (ºC)	$T_{d\text{-}5\%}$ (ºC)	$T_{g\text{-}DMTA}$ (ºC)	E'_R (MPa)	v_c (mmol cm^{-3})	E (MPa)	ε_b (%)	σ (S m^{-1})
AESO	3	312	26	26	3.04	93.9 ± 0.2	6.6 ± 1.4	8.84 × 10^{-12}
AESO + 1 wt.% rGO	3	310	17	20	2.34	94.5 ± 2.8	6.2 ± 0.1	8.40 × 10^{-12}
AESO + 2 wt.% rGO	-2	307	8	16	1.87	81.5 ± 3.7	7.2 ± 0.9	2.24 × 10^{-11}
AESO + 3 wt.% rGO	-3	307	4	17	1.99	58.5 ± 1.1	5.7 ± 0.2	2.26 × 10^{-10}
AESO + 4 wt.% rGO	-4	306	0	15	1.75	39.1 ± 0.2	4.7 ± 1.3	1.79 × 10^{-6}
AESO + 5 wt.% rGO	-8	295	-	-	-	-	-	6.32 × 10^{-3}
AESO + 6 wt.% rGO	-9	290	-	-	-	-	-	0.13

3. Conclusions

This work demonstrates the preparation of photocurable bio-based piezoresistive and thermoresistive materials by the combination of AESO and rGO as filler for filler contents up to 6 wt.%. It is observed that the addition of rGO to AESO hinders the curing process due to the light absorption by the filler that competes with the photoinitiator. However, the double bond conversions obtained are always above 50%. The addition of rGO induces a decrease on the cross-linking degrees down to 1.75 mmol·cm^{-3}. In addition, the rGO dispersion within the AESO polymer shows filler agglomerations and polymer voids that increases when rGO content increases, but without a high influence on the thermal stability or in the T_g. Mechanical properties are negatively affected by the addition of high rGO contents as indicated by a decrease of the E values. The electrical conductivity as a function of filler content shows a percolation threshold about 4 wt.% rGO content. Piezoresistive and thermoresistive responses have been evaluated for the 6 wt.% rGO content sample, the GF values being between 20 and 26 depending on the applied deformation, and stabilizing in values about 9 after repeated cycling. Further, thermoresistive sensibility values as high as 0.43 are obtained. Thus, this study demonstrates the important achievements and potentiality to obtain UV curable smart sensing materials starting from vegetable oil as bio-renewable resources of the polymeric matrix.

4. Experimental Methods

Materials: Acrylated epoxidized soybean oil (AESO) that contains 4,000 ppm of monomethyl ether hydroquinone as inhibitor was purchased from Sigma Aldrich and used as received. Phenyl bis(2,4,6-trimethylbenzoyl) phosphine oxide, also named as Irgacure 819 or BAPO, was purchased from BASF and used as photoinitiator. Ethanol (EtOH), from Merck, with 96% of purity was used as diluent. Reduced graphene oxide (rGO) with 1 nm thickness per layer and a flake size of 5 μm was acquired from LayerOne, previously Abalonyx, and used as conductive filler. This rGO is annealed at 1100 ºC, presents a surface area of 300-350 m^2 g^{-1}, an apparent density of 0.038-0.041 g cm^{-3} and an electrical conductivity of the powder compacts of 7 S cm^{-1}. Poly(ethylenglycol) diacrylate, PEGDA, with a molecular weight of 575 g mol^{-1} was purchased from Sigma Aldrich and used as sacrificial materials during 3D printing process, together with a 1 wt.% of Irgacure 819.

Sample preparation: AESO was initially mixed with ethanol (10 wt.%) in order to decrease its high viscosity, and 1 wt.% of Irgacure 819 photoinitiator was added. A homogeneous solution is obtained after magnetic stirring for 30 min at 50ºC. Then, the corresponding amount of carbonaceous filler was added to obtain samples with a rGO concentration range from 0 to 6 wt.%. To promote a good dispersion and disentanglement of rGO, the samples were

homogenized using an IKA T10 basic ULTRA-TURRAX equipment at 10,000 rpm during 5 min at room temperature (RT). Then, samples were magnetically stirrer for another 1 hour at 50ºC, followed by sonication during 2 hours in an ultrasound bath in order to degas the liquid materials. After complete dissolution, films were prepared by coating each formulation on a glass slide and curing them by illumination with a Dymax ECE 5000-UV lamp during 90 s at 130 mW cm^{-2} of irradiance. The resulting composite films showed thicknesses between 80 and 200 μm.

Photorheology: Real-time photorheology was evaluated an Anton PAAR Modular Compact Rheometer (Physica MCR 302, Graz, Austria). The tests were carried out in parallel-plate configuration with quartz bottom plate and a 25 mm diameter upper disk with a distance between them of 200 μm. The measurements were performed at constant frequency of 1 Hz and maintaining the sample at 25ºC while UV light generated by a Hamamatsu LC8 lamp irradiates the sample from the bottom part at 30 mW cm^{-2} of irradiance. The light was switched on after 60 s to let the system stabilize before the onset of the photopolymerization process. The averaged results of each sample after three measurements are presented.

Attenuated total Reflectance-Fourier Transform Infrared Spectroscopy (ATR-FTIR): ATR-FTIR equipment was used for the monitoring of the photocuring reaction by the disappearance of the acrylic double bond peak at 1630 cm^{-1}. For that, AESO/rGO samples were measured, first liquid samples (pre-cured), and then, irradiated samples (post-cured), using Thermo Scientific Nicolet iS50 FTIR Spectrometer equipped with a diamond crystal ATR accessory. The post-cured samples are obtained after 90 s irradiation at room temperature and under nitrogen atmosphere using a Dymax ECE 5000 UV lamp (130 mW cm^{-2} of irradiance). For each measurement, 32 spectra were obtained in the spectral range from 4000 to 600 cm^{-1} with a resolution of 4 cm^{-1}.

Scanning Electron Microscopy (SEM): rGO dispersion in the composite films was studied in the cross-section images of the cold fractured samples using Hitachi S-4800 microscope at an accelerating voltage of 5 kV with a magnification of 300, 1000 and 3000×. In all cases, samples were coated with a 20 nm gold layer by sputtering with a Polaron SC502 apparatus.

Thermogravimetric analysis (TGA): Film composite samples was characterized using a TGA equipment from Mettler Toledo model TGA/SDTA 851e. The measurements were carried out from 25 to 700ºC at a heating rate of 10 °C min^{-1} under nitrogen atmosphere (50 mL min^{-1}). The onset degradation temperature ($T_{d\text{-}5\%}$) was obtained at the temperature of 5 % mass loss.

Differential scanning calorimeter (DSC): The DSC analysis was performed with a Mettler Toledo DSC-1 equipment using a test method based on two heating scans and one cooling scan.

The first heating scan was from -60 to 200ºC and then the temperature was held at 200 ºC for 5 min in order to stabilize the sample. After that, the chamber was cooled down to -60 ºC and stabilized for 5 min. Finally, a second scan from -60 to 200 ºC was carried out. All heating and cooling rates were at 20 ºC min^{-1} and experiments were carried out under nitrogen atmosphere with a flow rate of 20 mL min^{-1}.

DLP – 3D printing: Rectangular samples with dimensions of 20 mm × 5 mm × 250 µm were prepared by 3D printing (Asiga MAX X27 DLP printer, XY pixel resolution of 27 µm; diode source emitting at 405 nm and building volume of 51.8 × 29.2 × 75 mm). In the printing process, silicon oil in vat surface is used as well as a sacrificial PEGDA base (around 50 µm of thickness) to avoid the adhesion and to easy-remove the printed samples. The layer thickness and the light intensity were fixed at 50 µm and 40 mW cm^{-2}. The exposure time was selected specifically for each formulation attending to the photorheology results. Printed samples were washed in EtOH bath under ultrasonication for 5 min and post-cured 3 min under UV-light of 12 mW cm^{-2} of irradiance provided by a Robot Factory medium-pressure mercury lamp.

Dynamic mechanical thermal analysis (DMTA): Rectangular 3D printed samples were used for the thermo-mechanical characterizations. DMTA measurements were performed using a Tritec 2000 DMA equipment from Triton Technology Ltd setting a temperature ramp of 2ºC min^{-1}, at a frequency of 1 Hz and with a total displacement of 20 µm. The apparent cross-linking density (ν_c) was calculated from the storage modulus values at the rubbery plateau (E'_R), obtained from graph at a temperature of 50ºC above the glass transition temperature and applying Equation 1:

$$\nu_c = \frac{E'_R}{3RT} \quad (1)$$

where ν_c is the cross-linking density in number of moles of network chains per unit volume of the network, R is the gas constant and T the absolute temperature (i. e., at T_g + 50 ºC).

Stress-Strain measurements: The stress-strain mechanical characteristics of the composites were evaluated in specimens with dimensions of about 30 mm x 10 mm of area (length x width) and thickness between 120 and 160 µm. Tensile tests were performed at laboratory conditions (about 22ºC) using a universal test machine Shimadzu model AG-IS (50 N load cell) at 1 mm min^{-1} of strain rate. The Young modulus (E), obtained by calculating the slope of the linear region, and the strain at break (ε_b) are provided as the average of three measurements for each sample with a deviation of less than 5% in all cases.

Electrical conductivity: The electrical conductivity (σ) of the composites was obtained with an automated Keithley 487 picoammeter/voltage source by measuring the voltage/current (I-V) curves applying voltages between -10 to +10 V with a step of 1 V. The volumetric electrical conductivity was calculated from the linear slope of the I-V curves. Previously, the composites

were gold-coated using a magnetron sputtering (Polaron SC502) with round contacts of 5 mm of diameter deposited in both sides of the samples. The electrical conductivity was determined from the obtained resistance (R) and the geometrical characteristics of the samples, following Equation 2:

$$\sigma = \frac{1}{R} \times \frac{l}{A} \quad (2)$$

where A is the area of electrodes and l the thickness of the composites.

The percolation theory of electrical conductivity as a function of filler content allows the determination of the percolation threshold for the composites according to Equation 3:

$$\sigma = \sigma_0(\varphi - \varphi_c)^t \quad (3)$$

where σ_0 is the conductivity of the filler (rGO in this case), φ is the filler content (in volume fraction), φ_c is the filler concentration at the percolation threshold and t is a universal exponent that indicates the dimensionality of the conductive system.[63,64]

Piezoresistivity: Piezoresistive tests were carried out by measuring, synchronously, the mechanical strain applied to the composites (universal test machine Shimadzu model AG-IS with a 50 N load cell) and the electrical resistance (Agilent 34401A multimeter). Test were performed under uniaxial stress-strain mechanical solicitations, having the samples similar geometry of those of the mechanical tests. Under uniaxial strain, the electrical resistance variations were measured by placing two conductive contacts on the surface of the samples, inside the deformation claws. To assure proper electrical connection, the contacts were painted using silver ink (Agar Scientific AGG3790) over the width of the film samples (10-30 mm distanced). The piezoresistive test were performed at deformations from 0.1 to 2 mm using strain rates of 0. 1 and 0.5 mm min^{-1}. More details on the experimental procedure can be found in the following reference.[34]

The gauge factor (GF) was used to quantify the electro-mechanical sensitivity of the samples, and it was calculated after Equation 4:

$$GF = \frac{dR/R_0}{dl/l_0} = \frac{d\rho/\rho_0}{dl/l_0} + 1 + 2\nu \quad (4)$$

where R_0 is the electrical resistance value of the composite without deformation, dR is the resistance variation when the material suffers a deformation dl.

Thermoresistivity: The thermoresistive effect of the composites was measured using a digital multimeter Agilent 34401A synchronized with a Linkam THMSE600 temperature oven. The measurements were performed in the AESO/rGO 6 wt.% filler content samples. Conductive silver ink (Agar Scientific AGG3790) was used as conductive electrode and contact to the multimeter was performed with copper wire. The heating-cooling profile was divided into 4

different cycles between 25 and 50 ºC. The thermoresistive sensitivity (S) was determined according to Equation 5:

$$S = \frac{\Delta R/R_0}{\Delta T} \times 100 \quad (5)$$

where ΔR and R_0 are the electrical resistance variation and the initial resistance, respectively, and ΔT is the temperature variation (in ºC).

Supporting Information

Supporting Information is available from the Wiley Online Library or from the author.

Acknowledgements

Financial support from the Basque Government Education (POSB_2020_1_0002) and Industry (Elkartek program) Departments are acknowledged. This work was also supported by the Portuguese Foundation for Science and Technology (FCT) in the framework of the strategic funding UID/FIS/04650/2021. P.C. acknowledges support from FCT by SFRH/BPD/110914/2015 grant. Technical and human support provided by SGIker (UPV/EHU, MICINN, GV/EJ, EGEF and ESF) is gratefully acknowledged. LayerOne, previously Abalonyx, is also acknowledged for the kindly supply of the reduced graphene oxide materials.

Conflict of Interest

The authors declare no conflict of interest.

Data Availability Statement

Research data are not shared.

Keywords

Bio-based resins, Reduced graphene oxide, Polymer composites, UV-curing, Piezoresistive

Received: ((will be filled in by the editorial staff))
Revised: ((will be filled in by the editorial staff))
Published online: ((will be filled in by the editorial staff))

References

[1] E. B. Murphy, F. Wudl, *Prog. Polym. Sci.* **2010**, *35*, 223.

[2] L. Da Xu, E. L. Xu, L. Li, *Int. J. Prod. Res.* **2018**, *56*, 2941.

[3] G. S. Hura, A. K. Singh, L. S. Hoe, *Advances in Communication and Computational Technology*, Springer, Singapore, **2020**.

[4] M. Javaid, A. Haleem, S. Rab, R. Pratap Singh, R. Suman, *Sensors Int.* **2021**, *2*, 100121.

[5] N. Y. Philip, J. J. P. C. Rodrigues, H. Wang, S. J. Fong, J. Chen, *IEEE J. Sel. Areas Commun.* **2021**, *39*, 300.

[6] S. Bhattacharya, A. K. Agarwal, O. Prakash, S. Singh, *Sensors for Automotive and Aerospace*, Springer, Singapore, **2018**.

[7] E. Llobet, *Sensors Actuators, B Chem.* **2013**, *179*, 32.

[8] S. Li, A. Simonian, B. A. Chin, *Electrochem. Soc. Interface* **2010**, *19*, 41.

[9] S. Cichosz, A. Masek, M. Zaborski, *Polym. Test.* **2018**, *67*, 342.

[10] T. Nardi, M. Sangermano, Y. Leterrier, P. Allia, P. Tiberto, J. A. E. Månson, *Polymer (Guildf).* **2013**, *54*, 4472.

[11] J. Oliveira, V. Correia, H. Castro, P. Martins, S. Lanceros-Mendez, *Addit. Manuf.* **2018**, *21*, 269.

[12] C. Mendes-Felipe, J. Oliveira, I. Etxebarria, J. L. Vilas-Vilela, S. Lanceros-Mendez, *Adv. Mater. Technol.* **2019**, *4*, 1.

[13] A. B. Kousaalya, B. Ayalew, S. Pilla, *ACS Omega* **2019**, *4*, 21799.

[14] M. Smol, P. Marcinek, J. Duda, D. Szołdrowska, *Resources* **2020**, *9*, 1.

[15] L. Fertier, H. Koleilat, M. Stemmelen, O. Giani, C. Joly-Duhamel, V. Lapinte, J. J. Robin, *Prog. Polym. Sci.* **2013**, *38*, 932.

[16] C. Noè, L. Iannucci, S. Malburet, A. Graillot, M. Sangermano, S. Grassini, *Macromol. Mater. Eng.* **2021**, *306*, 1.

[17] Y. Zhu, C. Romain, C. K. Williams, *Nature* **2016**, *540*, 354.

[18] C. Zhang, T. F. Garrison, S. A. Madbouly, M. R. Kessler, *Prog. Polym. Sci.* **2017**, *71*, 91.

[19] S. N. Khot, J. J. Lascala, E. Can, S. S. Morye, G. I. Williams, G. R. Palmese, S. H. Kusefoglu, R. P. Wool, *J. Appl. Polym. Sci.* **2001**, *82*, 703.

[20] E. Skliutas, M. Lebedevaite, S. Kasetaite, S. Rekštytė, S. Lileikis, J. Ostrauskaite, M. Malinauskas, *Sci. Rep.* **2020**, *10*, 1.

[21] M. Lebedevaite, J. Ostrauskaite, E. Skliutas, M. Malinauskas, *Polymers (Basel).* **2019**, *11*, 116.

[22] M. Lebedevaite, V. Talacka, J. Ostrauskaite, *J. Appl. Polym. Sci.* **2021**, *138*, DOI 10.1002/app.50233.

[23] C. Mendes-Felipe, A. Garcia, D. Salazar, J. L. Vilas-Vilela, S. Lanceros-Mendez, *Compos. Part C Open Access* **2021**, *5*, 100143.

[24] A. Madhi, B. S Hadavand, *J. Compos. Mater.* **2020**, *54*, 101.

[25] A. M. Díez-Pascual, A. L. Díez-Vicente, *J. Mater. Chem. B* **2015**, *3*, 4458.

[26] Y. Wu, C. Li, T. Chen, R. Qiu, W. Liu, *Compos. Part A Appl. Sci. Manuf.* **2022**, *152*, 106676.

[27] P. D. Desai, R. N. Jagtap, *ACS Omega* **2021**, DOI 10.1021/acsomega.1c04566.

[28] S. D. Vacche, A. Vitale, R. Bongiovanni, *Molecules* **2019**, *24*, DOI 10.3390/molecules24213858.

[29] Y. Zhang, H. Chen, S. Liu, L. Josien, G. Schrodj, A. Simon-Masseron, J. Lalevée, *Macromol. Mater. Eng.* **2021**, *306*, 1.

[30] Y. Guo, X. Wei, S. Gao, W. Yue, Y. Li, G. Shen, *Adv. Funct. Mater.* **2021**, *2104288*, 1.

[31] C. Li, E. T. Thostenson, T. W. Chou, *Compos. Sci. Technol.* **2008**, *68*, 1227.

[32] A. S. Alshammari, *Carbon-Based Polymer Nanocomposites for Sensing Applications*, Elsevier Inc., Oxford, UK, **2018**.

[33] M. Franco, R. Alves, N. Perinka, C. Tubio, P. Costa, S. Lanceros-Mendéz, *ACS Appl. Electron. Mater.* **2020**, *2*, 2857.

[34] P. Costa, J. R. Dios, J. Cardoso, J. J. Campo, C. R. Tubio, B. F. Gon alves, N. Castro, S. Lanceros-Méndez, *Smart Mater. Struct.* **2021**, *30*, DOI 10.1088/1361-665X/ac0cbe.

[35] W. Zhao, Z. Wang, J. Zhang, X. Wang, Y. Xu, N. Ding, Z. Peng, *Adv. Mater. Technol.* **2021**, *6*, 1.

[36] A. Cortés, A. Cosola, M. Sangermano, M. Campo, S. González Prolongo, C. F. Pirri, A. Jiménez-Suárez, A. Chiappone, *Adv. Funct. Mater.* **2021**, *2106774*, 1.

[37] C. Mendes-Felipe, J. Oliveira, P. Costa, L. Ruiz-Rubio, A. Iregui, A. González, J. L. Vilas, S. Lanceros-Mendez, *Eur. Polym. J.* **2019**, *120*, 109226.

[38] M. Martin-Gallego, R. Verdejo, M. A. Lopez-Manchado, M. Sangermano, *Polymer (Guildf).* **2011**, *52*, 4664.

[39] W. Liu, M. en Fei, Y. Ban, A. Jia, R. Qiu, *Polymers (Basel).* **2017**, *9*, DOI 10.3390/polym9100541.

[40] H. Pelletier, N. Belgacem, A. Gandini, *J. Appl. Polym. Sci.* **2006**, *99*, 3218.

[41] P. Costa, S. Gonçalves, H. Mora, S. A. C. Carabineiro, J. C. Viana, S. Lanceros-Mendez, *ACS Appl. Mater. Interfaces* **2019**, *11*, 46286.

[42] R. Brito-Pereira, C. R. Tubio, P. Costa, S. Lanceros-Mendez, *Compos. Sci. Technol.* **2021**, *213*, 108892.

[43] P. Cardoso, J. Silva, D. Klosterman, J. A. Covas, F. W. J. van Hattum, R. Simoes, S. Lanceros-Mendez, *Compos. Sci. Technol.* **2012**, *72*, 243.

[44] H. Lorenz, J. Fritzsche, A. Das, K. W. Stöckelhuber, R. Jurk, G. Heinrich, M. Klüppel, *Compos. Sci. Technol.* **2009**, *69*, 2135.

[45] B. Dong, Y. Yuan, J. Luo, L. Dong, R. Liu, X. Liu, *Prog. Org. Coatings* **2018**, *118*, 57.

[46] M. Sangermano, S. Marchi, L. Valentini, S. B. Bon, P. Fabbri, *Macromol. Mater. Eng.* **2011**, *296*, 401.

[47] A. Chiappone, I. Roppolo, E. Naretto, E. Fantino, F. Calignano, M. Sangermano, F. Pirri, *Compos. Part B Eng.* **2017**, *124*, 9.

[48] L. E. Nielsen, R. F. Landel, *Mechanical Properties of Polymers and Composites*, Marcel Dekker, Inc, New York, **1993**.

[49] K. Bandzierz, L. Reuvekamp, J. Dryzek, W. Dierkes, A. Blume, D. Bielinski, *Materials (Basel).* **2016**, *9*, DOI 10.3390/MA9070607.

[50] M. Martin-Gallego, M. Hernández, V. Lorenzo, R. Verdejo, M. A. Lopez-Manchado, M. Sangermano, *Polymer (Guildf).* **2012**, *53*, 1831.

[51] C. Mendes-Felipe, J. C. Barbosa, S. Gonçalves, N. Pereira, C. M. Costa, J. L. Vilas-Vilela, S. Lanceros-Mendez, *Compos. Sci. Technol.* **2020**, *199*, DOI 10.1016/j.compscitech.2020.108363.

[52] L. Dan, A. L. Elias, *Adv. Healthc. Mater.* **2020**, *9*, 1.

[53] C. Bessaguet, E. Dantras, G. Michon, M. Chevalier, L. Laffont, C. Lacabanne, *J. Non. Cryst. Solids* **2019**, *512*, 1.

[54] P. Costa, J. Nunes-Pereira, J. Oliveira, J. Silva, J. A. Moreira, S. A. C. Carabineiro, J. G. Buijnsters, S. Lanceros-Mendez, *Compos. Sci. Technol.* **2017**, *153*, 241.

[55] P. Costa, J. Oliveira, L. Horta-Romarís, M. J. Abad, J. A. Moreira, I. Zapiráin, M. Aguado, S. Galván, S. Lanceros-Mendez, *Compos. Sci. Technol.* **2018**, *168*, 353.

[56] A. Ferrreira, J. G. Rocha, A. Ansón-Casaos, M. T. Martínez, F. Vaz, S. Lanceros-Mendez, *Sensors Actuators, A Phys.* **2012**, *178*, 10.

[57] V. Eswaraiah, K. Balasubramaniam, S. Ramaprabhu, *Nanoscale* **2012**, *4*, 1258.

[58] J. Lu, R. P. Wool, *Polym. Eng. Sci.* **2007**, *47*, 1469.

[59] E. Lysenkov, Y. Davydenko, *2020 IEEE 10th Int. Conf. "Nanomaterials Appl. Prop.* **2020**, 40.

[60] M. Cen-Puc, G. Pool, A. I. Oliva-Avilés, A. May-Pat, F. Avilés, *Compos. Sci. Technol.* **2017**, *151*, 34.

[61] M. Cen-Puc, A. I. Oliva-Avilés, F. Avilés, *Phys. E Low-Dimensional Syst.*

Nanostructures **2018**, *95*, 41.

[62] S. V. Morozov, K. S. Novoselov, M. I. Katsnelson, F. Schedin, D. C. Elias, J. A. Jaszczak, A. K. Geim, *Phys. Rev. Lett.* **2008**, *100*, 11.

[63] S. Kirkpatrick, *Rev. Mod. Phys.* **1973**, *45*, 574.

[64] D. Stauffer, A. Aharony, *Introduction to Percolation Theory*, Taylor & Francis, London, **1992**.

This work reports on photocurable bio-based composite materials obtained by the combination of acrylated epoxidized soybean oil and reduced graphene oxide. The addition of the fillers leads a large increase on the electrical conductivity at the percolation threshold, as well as to piezoresistive and thermoresistive responses compatible with the application of the photocurable bio-based materials as sensing materials.

Cristian Mendes-Felipe*, Pedro Costa, Ignazio Roppolo, Marco Sangermano, Senentxu Lanceros-Mendez

Bio-based Piezo- and Thermo-Resistive Photo-Curable Sensing Materials from Acrylated Epoxidized Soybean Oil

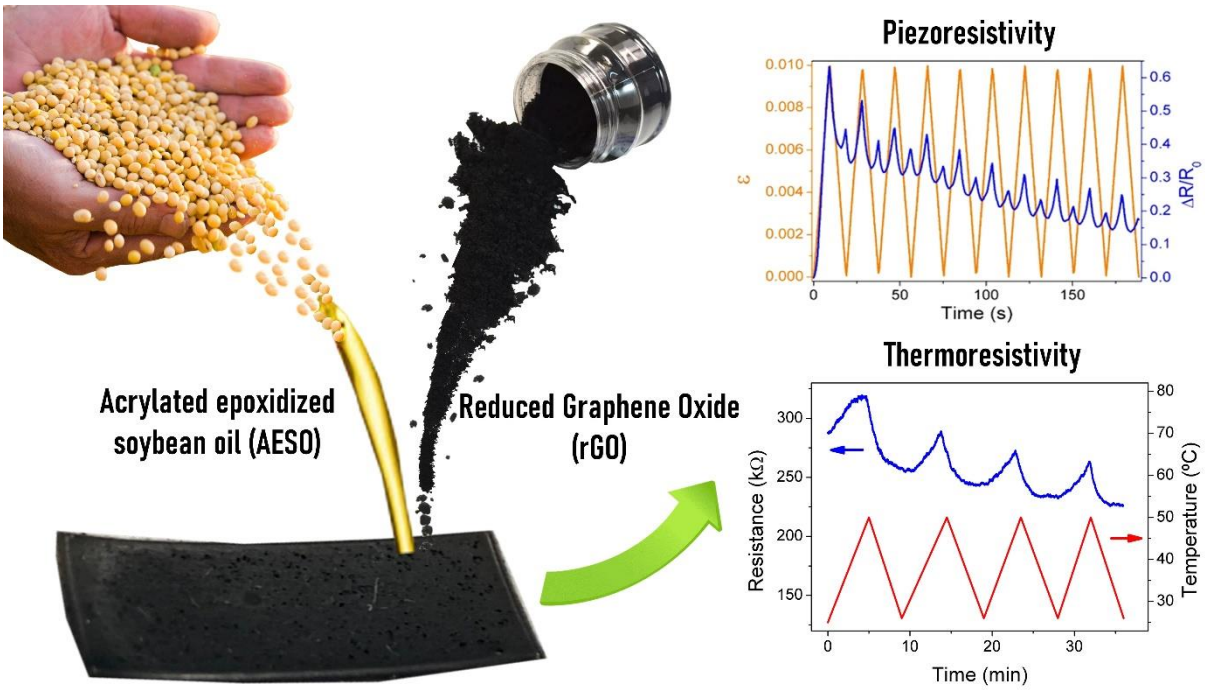

Supporting Information

Bio-based Piezo- and Thermo-Resistive Photo-Curable Sensing Materials from Acrylated Epoxidized Soybean Oil

Cristian Mendes-Felipe, Pedro Costa, Ignazio Roppolo, Marco Sangermano, Senentxu Lanceros-Mendez*

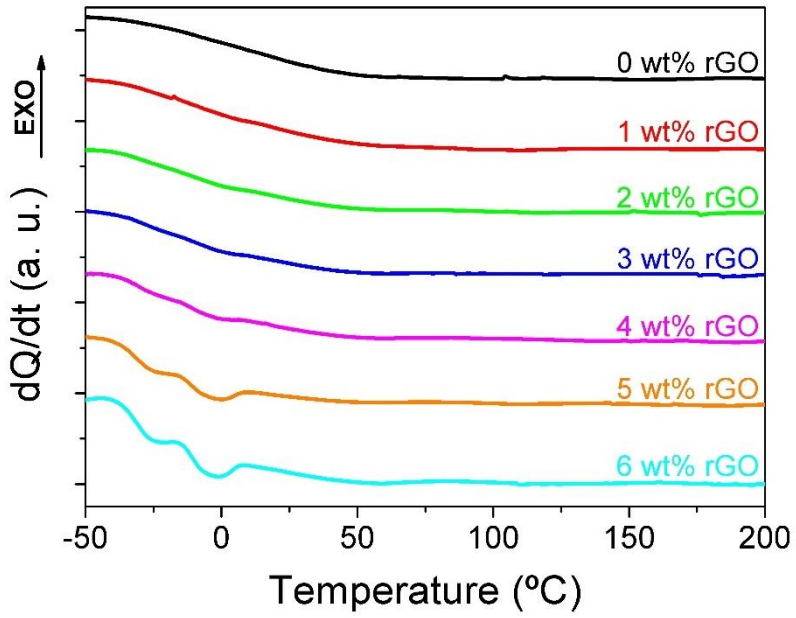

Figure S1. Differential scanning calorimetry (DSC) thermograms in the second scan for AESO neat polymer and AESO/rGO composites with rGO filler contents from 1 to 6 wt.%.

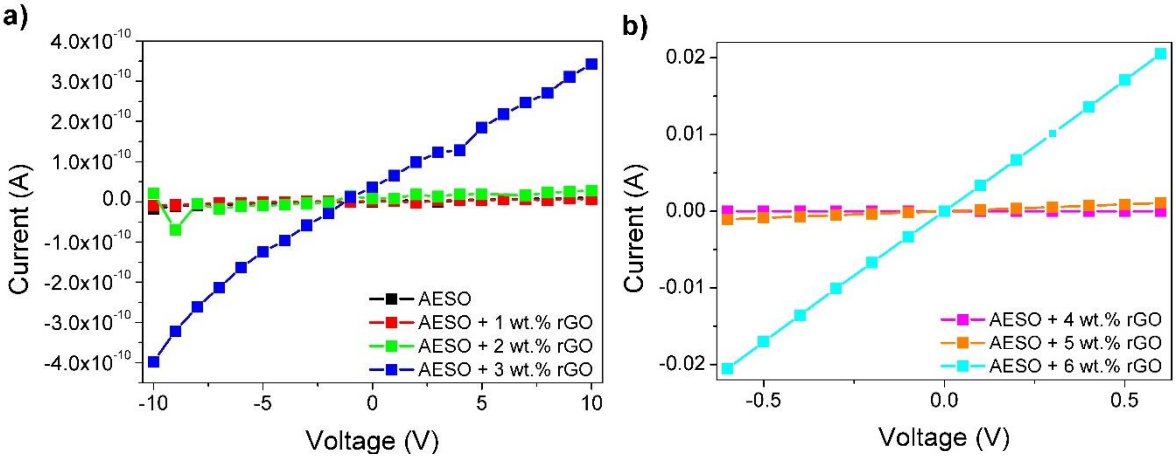

Figure S2. Current vs voltage (I–V) measurements of the AESO neat polymer and AESO/rGO composites from 1 to 3 wt.% rGO content (a) and from 4 to 6 wt.% rGO content (b).